scientific reports

Check for updates

OPEN

On the nature of nano twin-induced shear band formation in a dispersion strengthened copper alloy under micro-mechanical loading

Shadab Sarmast-Ghahfarokhi✉, Ali Ghatei-Kalashami, Adrian P. Gerlich, Michael J. Benoit & Y. Norman Zhou

A key challenge in metallic alloys with high ductility is understanding how microstructural inhomogeneities influence shear localization, leading to localized plastic deformation and material failure. In this study, we explore the phenomenon of shear localization in coarse-grained copper, a material traditionally regarded as having low susceptibility to such behavior. Contrary to conventional understanding, our findings reveal that microstructural inhomogeneities play a pivotal role in inducing extensive strain localization during low strain rate micro-mechanical loading. The presence of fine precipitate particles leads to strain localization at small strains and low strain rates by activating shear localization driven by void formation mechanisms. Furthermore, nanoscale precipitates act as sites for dislocation pile-up within deformed structures of shear bands, leading to the formation of nano twins within these bands. Consequently, precipitate particles serve a dual role: contributing to strain localization and potential cracking, while also enhancing the alloy's strength and ductility through nano-twinning mechanisms. This investigation offers a novel perspective on the interplay between material microstructure and deformation behavior, challenging existing paradigms in materials science.

Strain localization frequently occurs during plastic deformation of metallic materials, often leading to eventual failure[1]. This phenomenon arises from heterogeneous deformation at the dislocation scale, the most notable example of which is shear bands (SBs)[2–6]. Strain localization phenomena frequently occur in conjunction with thermal softening behavior in materials, which is indicated by a negative strain-hardening coefficient[4,7,8]. The Strain localization typically arises during severe plastic deformation processes or under dynamic loadings with high strain rates such as impact loading, shock peening, and low-temperature plastic deformation processes[1,9–11]. While it is believed that large plastic strain and high strain rate are typically precursors for the occurrence of SBs in many metallic systems, material properties, and microstructural characteristics can significantly change the material's susceptibility to strain localization[1,4], leading to the possibility of strain localization even under normal plastic deformation processes.

Materials with lower heat capacity and thermal conductivity are more prone to shear localization[7,8,12]. Additionally, microstructural features such as grain size and the presence of secondary phase particles play an important role in strain localization[1,13]. Metallic materials with small grain size structures are highly susceptible to SB formation due to their high work-hardening rate, driven by the grain boundary Hall-Petch strengthening mechanism, which results in low ductility and increased sensitivity to shear localization[1,14,15]. In face-centered cubic (FCC) alloys, shear localization strongly depends on the stacking fault energy (SFE) and grain size[1,4,16,17]. At high or medium SFE, SBs are formed during large plastic deformation and are associated with crystallographic textures such as Copper-type and Brass-type[18,19]. Conversely, adiabatic SBs can form in FCC alloys with low SFE and nanograin structures even under quasi-static loading[16].

Aside from grain size, microstructural inhomogeneities, such as the presence of secondary phase particles, can influence the formation of SBs[20–22]. However, the exact role of these particles in the deformation behavior remains unclear. For instance, studies have shown that precipitate particles can either hinder or promote the

Department of Mechanical and Mechatronics Engineering, University of Waterloo, 200 University Avenue West, Waterloo, ON N2L 3G1, Canada. ✉email: s2sarmast@uwaterloo.ca

formation and propagation of SBs in high-strength steels and copper alloys[19,20,22], depending on the precipitate size and aspect ratio throughout the matrix. It is unclear how the size, number density of precipitate particles, and their interaction with microstructural characteristics such as grain size affect the deformation mechanisms and shear localization sensitivity under specific loading conditions.

In this study, a coarse-grained copper (Cu) alloy containing precipitate particles ranging from a few micrometers to nanometers was subjected to micro-mechanical loading using a ball indentation technique. An extensive number of SBs were observed in the Cu alloy, particularly in areas far from the indented region with low plastic strain. The influence of microstructural inhomogeneities on the plastic deformation behavior of the Cu alloy was thoroughly investigated. It was observed that a sequence of plastic deformation mechanisms, from shear localization to deformation twinning, occurred during micro-mechanical loading. In each mechanism, the precipitate particles played a significant role. The micron-sized particles facilitated the formation of SBs through a micro-void formation mechanism, leading to shear localization around the particles. Once SBs with a high density of dislocations were formed, the presence of nanosized particles induced the formation of deformation nano-twins within the bands. The results showed that contrary to the belief that coarse-grained copper (CG) Cu alloys are less susceptible to shear localization and deformation twinning under applied micro-mechanical loading, microstructural inhomogeneities changed the threshold conditions for these phenomena to occur. This investigation challenges the prevailing understanding of how microstructure influences the deformation behavior of Cu alloys.

Results

Figure 1a shows the scanning electron microscopy (SEM) micrograph and electron backscatter diffraction (EBSD) map of the microstructure of the brazed bead, revealing the Cu matrix with an average grain size of $\sim$ 150 µm and uniformly distributed particles. The particles were formed as a result of the dilution of molten Cu filler material into the steel substrate during the brazing process and are referred to as precipitate particles[23,24]. Figure 1b presents a high-angle annular dark-field imaging (HAADF) image and corresponding energy-dispersive X-ray spectroscopy (EDS) elemental maps, revealing that the particles consist of iron (Fe), silicon (Si), and manganese (Mn). The presence of precipitate particles has been observed to result in the increase of the strength of the Cu-matrix[23].

Figure 1c depicts the load-depth (P–h) curve derived from the indentation test conducted in the brazed bead. Figure 1d,e show the SEM micrograph of the corresponding indentation where a pile-up of material and SBs are observed surrounding the circular indented area. The high-magnification SEM image (Fig. 1e) shows

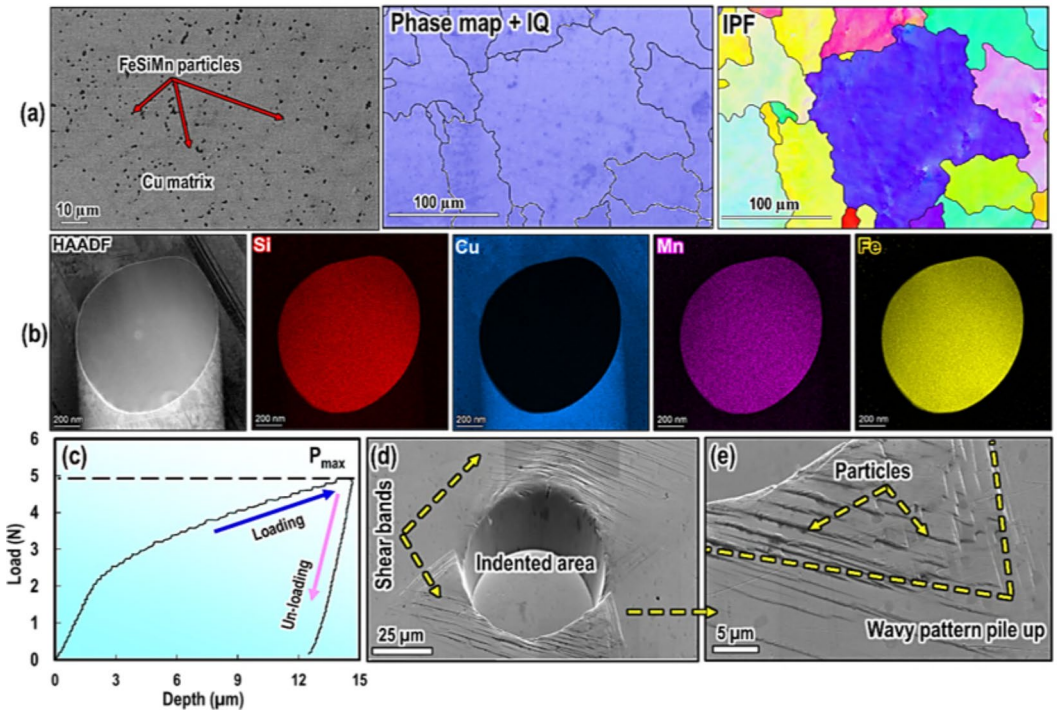

Fig. 1. (**a**) SEM micrograph along with image quality (IQ) and phase map as well as inverse pole figure (IPF) map of the brazed bead, revealing a Cu matrix with embedded particles, (**b**) HAADF image and corresponding EDS maps of the particles show that the particles are primarily composed of Fe, Si, and Mn, (**c**) Load-displacement ($P-h$) curve obtained from the indentation test, (**d**) 70° tilted SEM micrograph of the indentation area along with high magnification SEM micrograph of the pile-up and SBs formed surrounding the indentor, and (**e**) high magnification SEM micrograph showing pile-up and SBs formed around the indenter.

a wavy pattern within the pile-up, which indicates viscous flow caused by a temperature increase from plastic deformation (i.e., adiabatic heating), leading to the formation of such patterns[25]. Previous studies have mainly identified SBs within the pile-up region[26–28].

Figure 2(a)-1 and -2 shows an SEM micrographs illustrating the formation of multiple SBs in the region located far from the indentation area. The inclination angle of SB was measured at ∼30° with respect to the applied load utilizing an in-plane FIB micrograph as shown in Fig. 2(a)-3. The plastic zones were also examined using atomic force microscopy (AFM), as shown in Fig. 2(b)-1 and -2, which present two-dimensional (2D) and three-dimensional (3D) AFM images, respectively. The SB patterns and the corresponding line scan profile depicting of displacements caused by the indentation. The results revealed that each serration with a height difference of approximately 10–20 nm with respect to the matrix is indicative of a corresponding SB. This observation differs from the SBs observed in the previous literature, which were primarily confined to the region near the indented area and were radius or semi-circular bands[29–32].

The SBs were further investigated using EBSD analysis, as shown in Fig. 2c–f. The EBSD-IPF map (Fig. 2c,d) showed the presence of SBs within specific grains, each exhibiting consistent inclination angles. However, the inclination angles varied between two distinct grain orientations, influenced by the grain's orientation affecting deformation behavior[33]. This observation was confirmed with high magnification EBSD (Fig. 2d), revealing clear evidence of in-grain SBs with similar inclination angles. Plastic strain was evaluated using KAM calculations (Fig. 3e,f), indicating a relatively high degree of plastic strain within the SBs.

The characteristics exhibited by the SBs identified in this study are comparable to the bands formed during severe plastic deformation processes. These bands formed after severe plastic deformation typically appear narrow, ranging from approximately ∼5 to 200 µm wide, and their width increases as plastic strain is increased[1]. The bands are also separated from each other with a characteristic boundary with the matrix[10]. This type of SB is commonly observed under high strain rates or shock-hardening processes in Cu alloys[10,34,35]. Yet, the SBs observed in this study were formed by the application of a low but localized load[26,27,30,36], and in this condition, there will be high plastic strains generated at the edge of a nearly flat indenter[37]. This finding suggests that the Cu matrix is prone to shear localization during plastic deformation around an indentation.

Besides the alloy type, the investigated Cu alloy possesses a large grain size structure, typically resulting in low sensitivity to shear localization. Shear banding is less likely to typically occur in metals with larger grain sizes in both BCC or FCC structures[15,38,39]. Li et al.[40] showed that lower strain hardening coupled with higher thermal softening makes ultra-fine-grain titanium alloy more susceptible to shear localization. The same behavior has been observed in BCC iron during compressive loading where shear localization occurred in grain

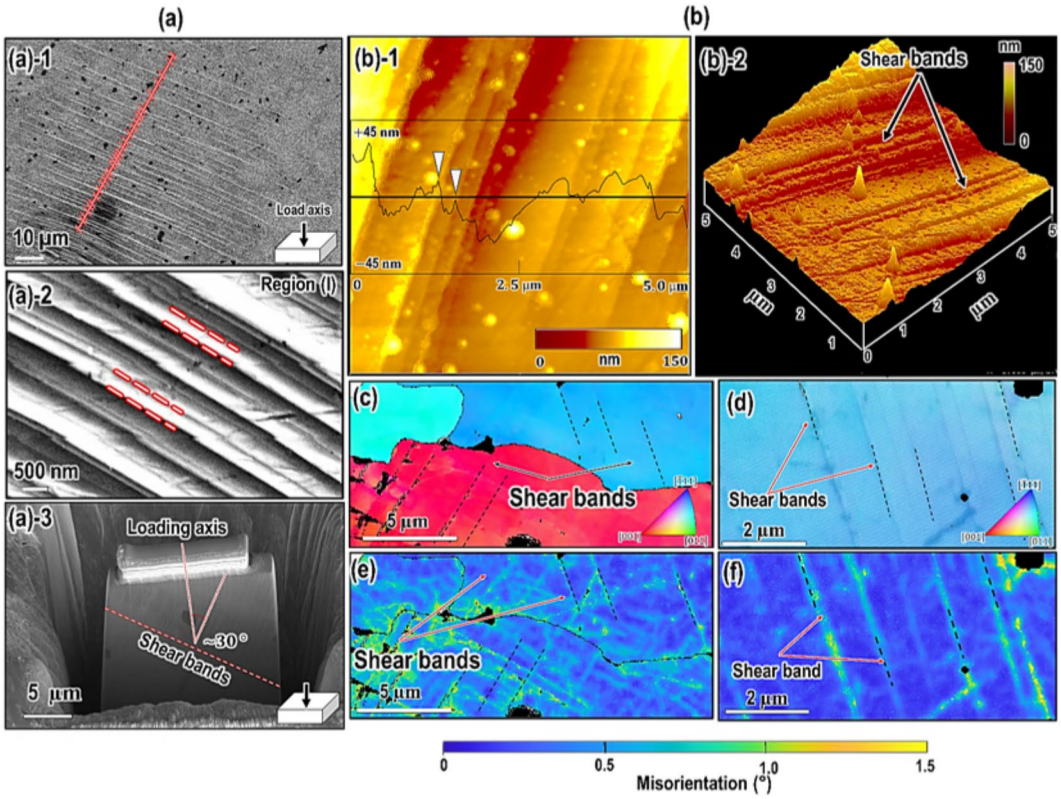

Fig. 2. (**a**) SEM micrograph of the indented area reveals the formation of shear bands, (**b**) 2D and 3D AFM images of shear bands and Cu matrix, (**c**) inverse pole figure maps showing the presence of shear bands within two distinct grains, (**d**) high magnification inverse pole figure map of in-grain shear bands and (**e**,**f**) the corresponding kernel average misorientation (KAM) of the shear bands.

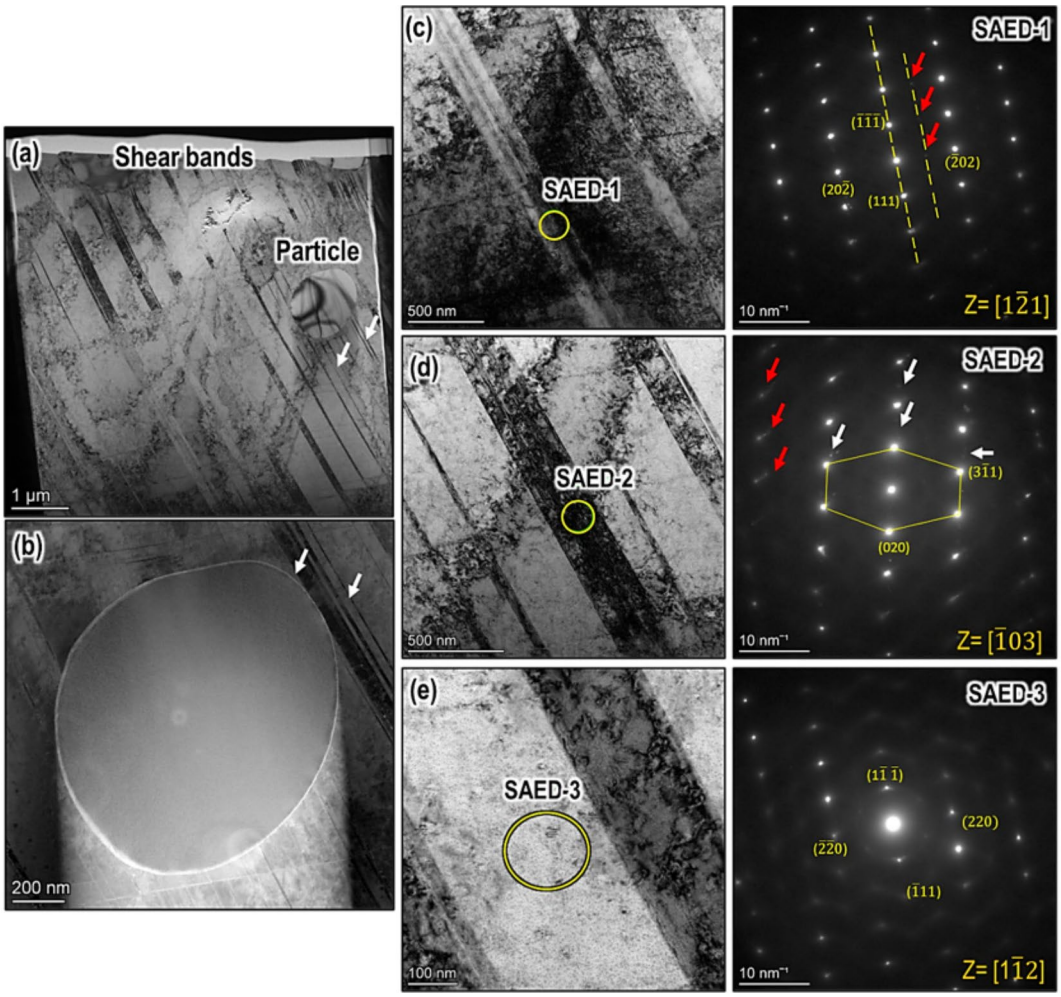

Fig. 3. (**a**) TEM micrographs of the SBs in the matrix and the vicinity of a precipitate particle, (**b**) High-magnification TEM image showing particle and shear bands formed in its vicinity, (**c**–**e**) TEM micrographs and corresponding SAED patterns at different locations, including a spot containing both an SB and matrix (**c**), within the SB (**d**) and the matrix (**e**) (for interpretation of the references to color in this figure, the reader is referred to the web version of this article).

sizes below 300 nm, even at quasi-static strain rates and low strains, and emerged as the dominant mode of plastic deformation[15]. These investigations revealed that the occurrence of SBs during low strain or strain rate conditions is confined to ultrafine or nanograin structures. This is in contrast with the current study, in which SBs were observed in a coarse grain (∼150 μm) Cu matrix. Furthermore, it has been shown that microstructural inhomogeneities, such as secondary phase particles, can significantly impact the formation of SBs[1]. Small carbide precipitates with high aspect ratios and volume fractions have been observed to be potential sites for the formation of SBs in steel, while micron-size particles were more resistant to the formation of SBs[22]. In contrast, it has been reported that Cu-rich nano-precipitates can effectively act as an absorber/of energy during impact loading and are thus capable of effectively preventing the formation of SB[20]. This suggests that the role played by precipitate particles is strongly dependent on their composition, size, and number density. Furthermore, the effect of all of these microstructural factors on SB formation varies depending on the loading conditions.

Figure 3a shows transmission electron microscopy (TEM) micrographs revealing a sequence of SBs exhibiting consistent inclination angles, indicative of in-grain SBs. Localized SBs, ranging in width from 20 to 300 nm, are visible in the TEM micrograph. Additionally, SBs formed near particles appear narrower and are situated closer together compared to those formed within the matrix, as illustrated by the high-magnification TEM image in Fig. 3b. The width of SBs is influenced by factors such as strain, strain rate, and the presence of precipitates[1,14]. Depending on the size of particles, their presence within the matrix can enhance localized strength, leading to increased strain localization and narrower SBs. Figure 3c–e show TEM micrographs and selected area electron diffraction (SAED) patterns at three locations, including a spot containing both SB and matrix (Fig. 3c), within SB (Fig. 3d) and within the Cu matrix (Fig. 3e). The bright spots in Fig. 3c were associated with the Cu matrix, while the faint small spots were observed at a distinct angle between the {111} spots. This suggested that the faint spots were caused by a periodic defect, resulting in a weak diffraction pattern appearing midway on the SB. One possible explanation for the faint spots observed in this SAED pattern is the presence of partial dislocations. In

FCC metals with low or medium SFE, the tendency for dislocation cross-slip is reduced, leading to an increased likelihood of dislocation pile-up. As a result, the dislocations extend into two partial dislocations with a stacking fault existing between them[41]. Figure 3d displays a TEM micrograph of SBs, where bright spots show the Cu matrix and faint spots indicated by white arrows indicate partial dislocations. Additionally, in Fig. 3d, there are spots marked by red arrows that split into two separate spots, suggesting the coexistence of nano twins within the SBs. Comparing the SAED patterns of the SB (Fig. 3d) with the matrix (Fig. 3e) showed that the SB exhibited a more diffuse pattern than that of the matrix. It is worth noting that the formation of a twin-coupled SB structure derives from intensive dislocation interactions triggered by plastic deformation and precipitate particles. As indentation induces localized deformation, plastic strain is applied beneath the indenter, leading to dislocation interactions induced by concentrated stress, as shown in previous work[37].

Typically, deformation twinning rarely occurs in CG FCC metals with medium to high SFE due to two primary reasons: (i) the number of independent slip systems, which render slip a dominant mode of deformation, and (ii) higher critical twinning stress in comparison to slip stress[42]. Experimental evidence indicates that deformation twinning in CG FCC materials occurs after substantial strain hardening, high strain rates, or during deformation at low temperatures[43], and is known to proceed through the well-known pole mechanism[42]. In this process, the prismatic dislocation undergoes dissociation into two partial dislocations $((a/2)[110] = (a/3)[11\bar{1}] + (a/6)[112])$ and extends by climbing a Shockley dislocation[42]. This progression requires a high critical resolved shear stress achievable only at very low temperatures or under high strain rates[42]. Most importantly, the critical twinning stress follows the Hall-Petch relationship[44], wherein the twinning stress significantly decreases with increasing grain sizes for materials with medium to low SFE[42]. It has been reported that twinning can occur in CG Cu within a grain size range of 117–311 μm[13]. In spite of this, it is still required to provide high strain or strain rate or deformation under low temperatures to meet the minimum stress required for twining. While the Cu matrix investigated in this study has a CG structure, the twining happened under low strain but localized indentation loading.

Figure 4a,b show high-resolution TEM analysis, of the presence of nano twins within the SBs. The corresponding fast Fourier transformation (FFT) diffractogram from the twin-coupled SB (Fig. 4(a)-1) further confirms the twin structure, as indicated by the red arrows in the diffractogram. A high-magnification TEM micrograph depicting the SBs, along with corresponding FFT diffractograms from both the matrix (FFT1) and the SB (FFT2), is presented in Fig. 4(a)-2. The overlaid image of the FFT diffractograms (Fig. 4(a)-3) indicates a misorientation of approximately 10° between the SB and the matrix, suggesting the presence of a low-angle grain boundary (LAGB) at the interface between the SB and the matrix. This observation aligns with findings from EBSD maps (Fig. 2) which showed the presence of in-grain SBs.

In addition, the TEM micrograph showed lattice fringes in certain regions of the SBs (Fig. 4(b)-1 and -2). The spacing of these lattice fringes was measured at approximately 0.17–0.25 nm. Moreover, the lattice fringes exhibited almost identical orientations at various locations within the SBs. The FFT diffractogram from the

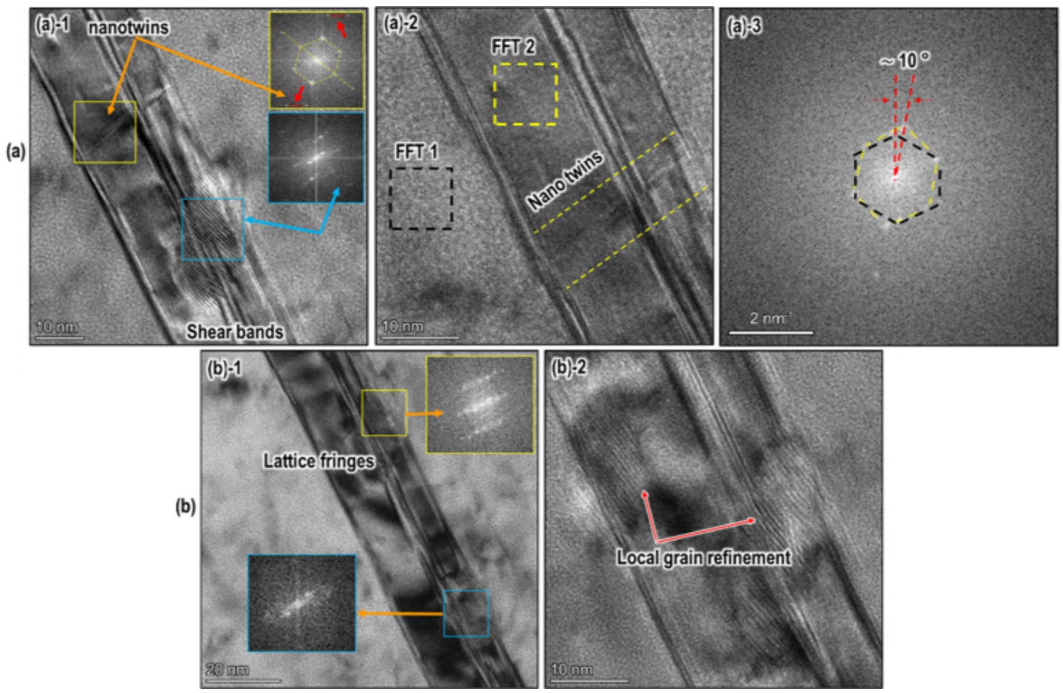

Fig. 4. (**a**) TEM micrograph alongside the fast Fourier transformation (FFT) diffractogram corresponding to the various regions in the shear band and matrix. The FFT diffractogram reveals two sets of diffraction spots corresponding to the nano twins within the SBs, (**b**) TEM micrographs of the lattice fringes within the shear band reveal local grain refinement, as evidenced by the multi-spot FFT diffractogram.

lattice fringes (Fig. 4(b)-1) indicated a multi-grain structure within the SBs, suggesting local grain refinement. The grain refinement usually happens as a result of recrystallization, a phenomenon that typically occurs in adiabatic SBs, where the high strain or strain rate causes thermal softening to prevail over work hardening[45,46]. It is noteworthy that these lattice fringes were observed only in specific local areas of the SBs[47]. This inhomogeneous characteristic of different microstructures within SBs is attributed to localized plastic deformation during micro-mechanical ball indentation loading[48,49].

Figure 5a shows a more detailed illustration of the formation of nanotwins within SBs. High-magnification TEM micrographs (Fig. 5(a)-1 and -2) and EDS analysis (Fig. 5b), coupled with FFT diffractograms (see Fig. 5(a)-3), provide further confirmation of the presence of nano twins. It is evident that the nano twins are confined to a small area within the SBs, as depicted by yellow arrows in the high-magnification TEM micrograph in Fig. 5(a)-3. It is well-known that the local stress required for nucleation of deformation twinning in FCC materials is high, typically ranging from 150 MPa for single crystal Cu to 300 MPa for Ni alloys[42]. To reach this high level of local stress, significant plastic deformation is generally required. Figure 5b shows the TEM/EDS analysis of the nano-sized precipitate particles, clearly demonstrating that they are composed of Si, Mn, and Fe, consistent with the composition of the micron-size particles observed in Fig. 1. The pre-existing SBs and the nano-sized Si-Fe-Mn precipitates contribute to lowering the critical stress necessary for the formation of deformation nanotwins in the studied CG Cu alloy.

Discussion

Experimental and analytical findings have consistently demonstrated that the instability criterion, where materials soften with increasing strain (i.e., $d\tau/d\gamma \leq 0$), is a necessary condition for shear strain localization and the formation of SBs[1]. Plastic deformation instabilities may arise during high strain rate deformation[11,50], or they can emerge from the specific geometry of the deforming sample[51,52], alongside factors related to the inhomogeneous microstructure, such as crystallographic texture or the presence of precipitate particles[1]. In the present study, shear localization and deformation nanotwinning were observed in coarse-grained Cu at room temperature and low strain rates during ball indentation loading, which had not been investigated previously. The sequence of plastic deformation processes is as follows: (i) an inhomogeneous and localized plastic strain distribution, with the substrate flowing around the sides of the indenter, resulting in pile-up with hardening effects, (ii) the formation of shear localization surrounding the plastic strain distribution around the indent area, and (iii) the formation of deformation nanotwins within the SBs.

Shear localization in CG cu matrix

Ultrafine and nanograin alloys are more prone to shear localization than CG structures, as smaller grain sizes exhibit limited strain-hardening due to reduced dislocation accumulation and generally low strain-rate sensitivity, resulting in shear localization during dynamic deformation[40]. However, this study showed that a CG Cu alloy can also exhibit shear localization during micromechanical loading. This tendency can be attributed to two key factors: (i) localized and inhomogeneous plastic deformation during ball indentation, and (ii) a heterogeneous microstructure, including dispersed precipitate particles within the Cu matrix.

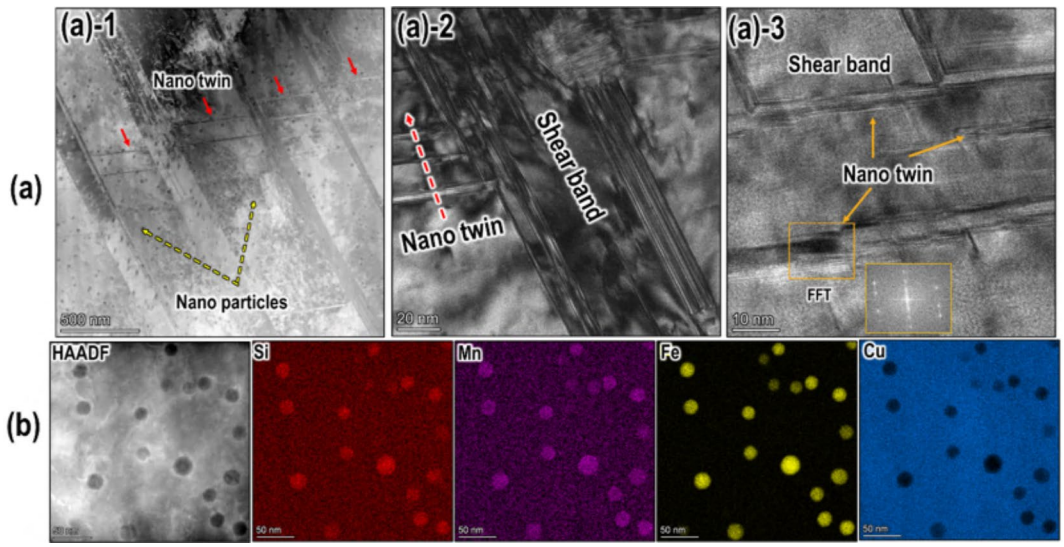

Fig. 5. (**a**) High-resolution TEM micrographs of the nano twins formed within the shear bands and the matrix. The TEM micrograph shows the presence of nano-sized precipitate particles within the matrix. (**a**)-2 and (**a**)-3 are high-magnification TEM micrographs from different regions of (**a**)-1, (**b**) EDS elemental maps of the nano-sized precipitates show that the particles have the same composition as the micron-size particles. The figure shows that the nano-sized precipitates may act as obstacles to dislocation motion, thereby increasing the pile-up of dislocations and further assisting in the formation of nano twins within the shear bands.

Deformation pile-ups and shear localization have been previously observed in nanocrystalline Fe under ball indentation due to localized and highly strained plastic deformation[48]. However, in earlier studies, SBs were typically confined to areas near the indentation tip[48]. In contrast, this study found that SBs propagated far from the indented area, extending into regions of low plastic strain, as indicated by finite element simulations of plastic strain distribution in previous work[37]. This extended SB formation is likely due to the heterogeneous microstructure, specifically the dispersion of precipitate particles.

Alloys with precipitates, impurities, or defects are highly susceptible to SB formation. For instance, it has been shown that precipitate carbides can act as nucleation sites for SBs where the size and density of these precipitates significantly affect susceptibility to shear localization[22]. One mechanism explaining this is based on microvoid formation during applied shear strain. Voids act as sources of geometric instability independent of any thermal softening mechanism[53]. Experimental evidence shows that dislocations interact with plastic strains around these particles, leading to the cooperative nucleation of voids, which ultimately cause shear instability and the formation of SBs. The nucleation of voids depends on the size, distribution, and aspect ratio of the precipitates, with large or closely spaced particles tending to nucleate voids at relatively low strains, accelerating the onset of shear localization[53]. A critical stress criterion model can be employed to correlate the influence of particle characteristics on micro-void formation. For materials with small interparticle spacing, the interfacial stress can be determined by Eq. (1)[54]:

$$\sigma_{rr} = K_0 \left[\left(\frac{\gamma}{\gamma_c} \right)^{1/n} + 3^{1/2} \left\{ \frac{3^{\frac{1}{2}} \left(\frac{\gamma}{\gamma_0} \right)}{\left(\frac{\lambda}{R} \right)} \right\}^{1/n} + \frac{6^{1/2} \lambda}{M \, R} \right] \tag{1}$$

where σ_{rr} is the interfacial tensile stress, K_0 is the yield stress in shear, γ is the shear strain, γ_0 is the shear strain at yield, n is the strain hardening exponent, M is the Taylor factor, λ is the interparticle spacing, and R is the particle radius. The ratio of $\frac{\lambda}{R}$is determined by the following equation[54]:

$$\frac{\lambda}{R} = \left(\frac{2}{3} \frac{\pi}{f_v} \right)^{1/2} - \left(\frac{8}{3} \right)^{1/2} \tag{2}$$

where f_v is the volume faction of particles. The model clearly illustrates how particle characteristics, such as size, interspacing, and volume fraction, affect the critical strain required for void nucleation. The critical interfacial stress for void nucleation depends on both the size and distribution of particles. With the same volume fraction (i.e., the same λ / R ratio), nano-sized particles allow for greater strains before void nucleation occurs. On the other hand, micron-size particles initiate voids at lower strains. This is consistent with the results presented in this study. The micron-size particles increase the probability of void formation, promoting shear localization, while nano-sized particles require higher strain for void formation[54].

Therefore, voids could initiate shear banding before reaching the critical shear strain for localization. However, void formation within the SB is typically delayed until some time after reaching the instability strain. Larger voids that are observed within SBs are thought to develop during the late stages of deformation, particularly during unloading when the material within the band still maintains a high temperature due to plastic deformation. As a result, voids are frequently observed within SBs in materials with low thermal conductivity, such as titanium alloys, but are not commonly found in steel or aluminum alloys[12] and Cu alloys.

Shear band-induced nano twining

During the process of severe plastic deformation, when the stress concentration resulting from dislocation pile up reaches the level of the critical twinning stress, deformation twinning might occur. Therefore, the local dislocation density, ρ_n for activating deformation twinning can be determined according to Eq. (3)[42]:

$$\rho_n = \frac{\gamma^2}{G^2 b_1^2} \times \frac{1}{\left(n \acute{\alpha} b - b_1 \right)^2} \tag{3}$$

where γ is SFE, and G is the shear modulus. For Cu alloy the $\gamma = 45 \times 10^{-3} J/m^2$, $G = 48.3\, GPa$, and the Burgers vector modulus of the full dislocation (b) being $\left(\frac{\sqrt{2}}{2} \right) a$, where the lattice parameter (a) is 3.6 $\times 10^{-10}$ m. The Burgers vector of the partial dislocations b_1, and b_1, being $\left(\frac{\sqrt{6}}{6} \right) a$. For a given value of $n = 2$ and an empirical material constant (ά) of 0.5, the dislocation density ρ_n is calculated as 3.4 $\times 10^{15}\, \mathrm{m}^{-2}$[42].

Based on the aforementioned equation, ρ_n can be used to calculate the local dislocation density required for activating deformation twinning. As SBs exhibit high dislocation density and a high degree of lattice distortion, as shown by TEM micrographs, the local dislocation density within SBs is sufficiently high to surpass the critical value needed to initiate the formation of deformation twins. It should be mentioned that nano twins were not observed in all SBs and were limited to some local areas of SBs. The TEM micrograph in Fig. 5a revealed the presence of nano-sized precipitate particles throughout the sample. The nano precipitates have the same composition as the micron-size particles shown in Fig. 1. Nanotwins are clearly observed in areas with the presence of nano-sized precipitate particles. This observation explains why nano twins form in specific regions of the SBs but are not present throughout all regions. The nano-sized precipitate particles act as obstacles to

dislocation movement, increasing dislocation entanglement and thereby promoting the activation of twin formation. A recent study using molecular dynamics (MD) simulations on FCC Cu showed that nanoprecipitates not only serve as obstacles but also generate dislocations due to the lattice mismatch between precipitate and matrix[55]. When the applied stress exceeds a critical level, dislocations nucleate and propagate, facilitating plastic deformation[55]. This dual functionality allows the material to maintain strength while deforming uniformly, thereby enhancing ductility. These dislocations may also trigger the formation of deformation twins.

Deformation mechanisms

Figure 6 illustrates the sequence of deformation mechanisms observed in the CG Cu alloy with dispersed precipitate particles ranging from a few micrometers to approximately 10 nm in the current study when subjected to localized deformation. Under ball indentation loading, the material exhibits substantial localized strain, resulting in a pile-up of material and a radial distribution of strain around the indentation area.

In this study, SBs are formed near the indentation region and propagate to areas farther from the indentation site. The SBs that formed away from the indentation region were further analyzed, as highlighted in Fig. 6. Stage 1 illustrates the microstructure of the CG Cu matrix, which contains both micron-size and nano-sized particles. In stage 2, following the microvoid formation mechanism, voids form within the micron-size particles, as they require less plastic strain for void formation. The growth of these voids leads to plastic strain instability, contributing to the formation of SBs. Once the SBs are formed, the high density of dislocations in the localized areas serves as preferred sites for dislocation pileups within the deformed SBs. In stage 4, the high dislocation density within the shear bands interacts with the nano-sized precipitate particles. This interaction reduces the critical strain threshold required for deformation twinning, which subsequently facilitates the formation of nanotwins within the SBs.

In the context of brazing high-strength steels, nanoparticles within the Cu matrix play a critical role. These particles act as effective dislocation barriers, thereby enhancing local strength and influencing the overall deformation behavior of the CG matrix. Nanoparticles facilitate nanotwin formation, a key mechanism that simultaneously improves strength and ductility[56–58]. However, the micron-size particles also contribute to shear localization in the form of SBs, potentially leading to premature failure. It is important to note that the particle size distribution can be controlled and tailored through process optimization, as demonstrated in our previous works[23,24]. This investigation is significant because failures in brazed joints often occur through brazed beads. Understanding the deformation mechanisms of the Cu matrix in brazed beads can lead to microstructure optimization, enhancing the mechanical integrity of brazed joints.

Methods

In this work, a brazed joint fabricated by using a Cu-based alloy (Cu-2.9Si-0.8Mn-0.02Fe, all in wt%) filler wire to join zinc-coated interstitial free (IF) steel sheets using the automatic robotic gas metal arc brazing process with a working angle of 25°, a push angle of 30°, and a wire feed speed of 350 in/min (8.89 m/min). The power supply was set to direct current electrode positive (DCEP) mode with surface tension transfer and travel speed of 30 in/min (760 mm/min). A more detailed description of the brazing process can be found in Refs[23,24].

The sample preparation was conducted utilizing the typical metallographic method in addition to a final vibratory polishing stage using a colloidal silica suspension for 30 min. Subsequently, each sample was loaded using an instrumented indentation tester (Nanovea M1) with a nearly flat tip indenter with a 50 µm diameter and a loading of 5 N. The test was conducted on at least five different points on the brazed bead, with a loading and unloading rate of 10 N/min. The load-depth (P–h) indentation curves were measured at room temperature.

The microstructure was characterized using SEM (Zeiss FESEM 1530), AFM (DI Nanoscope IV), and EBSD (JEOL JSM 7000f) imaging. EBSD data was analyzed using the MTEX toolkit in MATLAB[59]. To conduct site-specific TEM analysis, thin foil samples near the indented region containing shear bands were cut from the longitudinal sectional of the Cu-based alloy using FIB (Thermo Scientific Helios G4 PFIB machine) micro-machining. HAADF micrographs and EDS were captured using an FEI Titan 80-300HB operating at 300 keV.

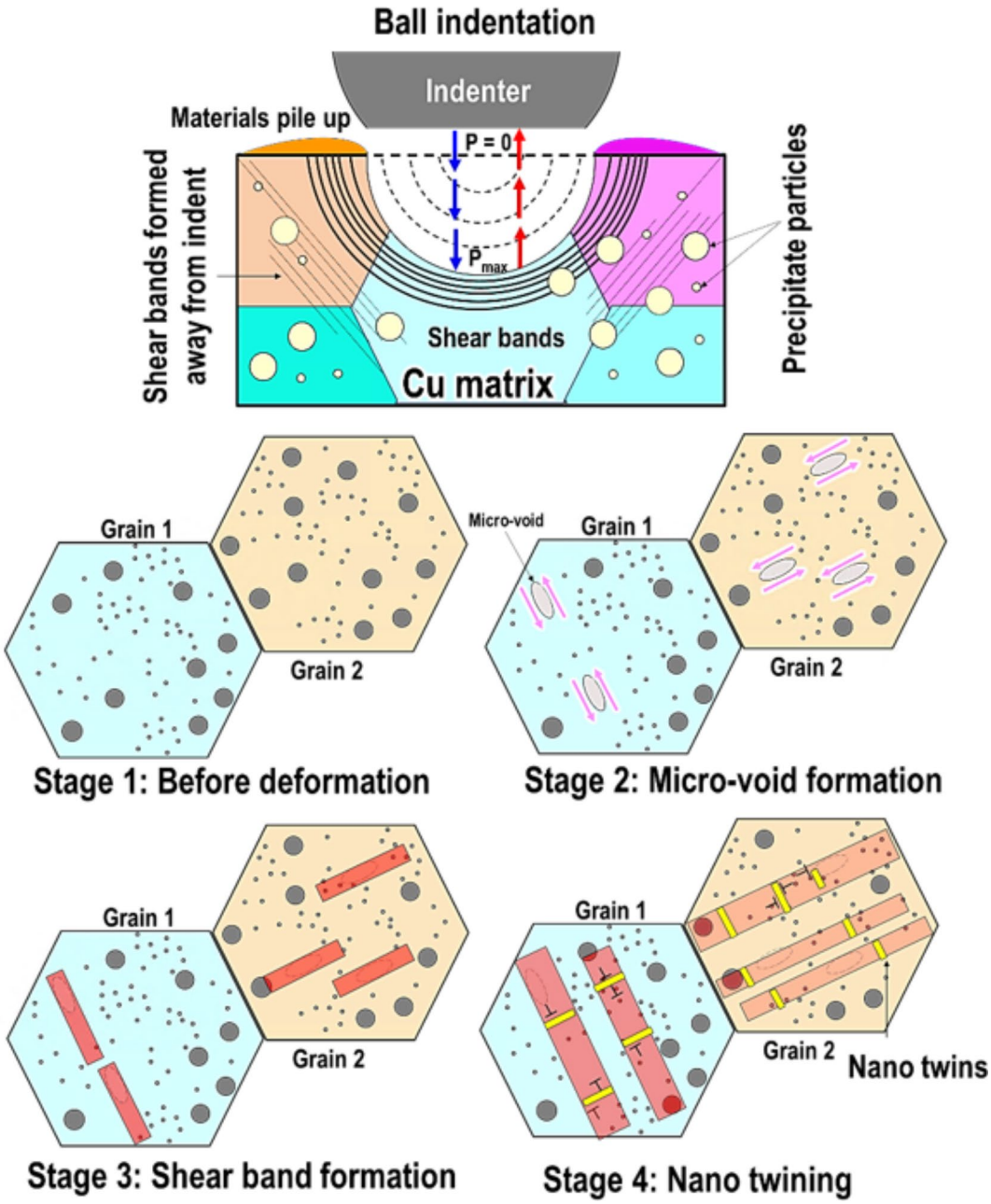

Fig. 6. Schematic representation showing the microstructural evolution of the precipitate-dispersed Cu matrix throughout distinct stages of plastic deformation; stage 1: The microstructure of the coarse-grained (CG) copper (Cu) alloy is characterized by a distribution of precipitate particles varying in size from several micrometers down to the nanometer scale. Stage 2: Shear localization occurs due to the formation of voids around the micron-size precipitate particles. Stage 3, The localized shear strains lead to the development of distinct shear bands. Stage 4: Within these shear bands, the high density of dislocations interacts with the nano-sized precipitate particles. This interaction reduces the critical strain required for deformation twinning, eventually resulting in the formation of nano twins within the shear bands.

Data availability

The datasets generated and/or analyzed during the current study are not publicly available due to ongoing projects but are available from the corresponding author upon reasonable request.

Received: 22 July 2024; Accepted: 23 September 2024
Published online: 08 October 2024

References

1. Yan, N., Li, Z., Xu, Y. & Meyers, M. A. Shear localization in metallic materials at high strain rates. *Prog. Mater. Sci.* **119**. https://doi.org/10.1016/j.pmatsci.2020.100755 (2021).
2. Hu, X., & Szlufarska, I. Amorphous shear bands in crystalline materials as drivers of plasticity. *Nat. Mater.* **22**, 1071–1077 (2023).
3. Wang, J. Wang, Y., Cai, W., Li, J., Zhang, Z., & Mao, S. X. Discrete shear band plasticity through dislocation activities in body-centered cubic tungsten nanowires. *Sci. Rep.* **8**, (2018).
4. Boakye-Yiadom, S. *Microstructural evolution of adiabatic shear bands in steel by impact*. (2014).
5. Weidner, A. *Springer Series in Materials Science 295 Deformation Processes in TRIP/TWIP Steels In-Situ Characterization Techniques*. http://www.springer.com/series/856.
6. Jang, T. J. Choi, W.S., Kim, D.W., Choi, G., Jun, H., Ferrari, A., Körmann, F., Choi, P.P. and Sohn, S.S. Shear band-driven precipitate dispersion for ultrastrong ductile medium-entropy alloys. *Nat. Commun.* **12** (2021).
7. Li, Z. Zhao, S., Alotaibi, S.M., Liu, Y., Wang, B. and Meyers, *M.A*, Adiabatic shear localization in the CrMnFeCoNi high-entropy alloy. *Acta Mater* **151**, 424–431 (2018).
8. Catastrophic *Thermoplastic Shear.* http://asmedigitalcollection.asme.org/appliedmechanics/article-pdf/31/2/189/5445990/189_1.pdf (1964).
9. Meyer, L. W. , & S. M. Critical adiabatic shear strength of low alloy steel under compressive loading (1986).
10. Andrade, U., Meyers, M. A., Vecchio, K. S. & Chokshi, A. H. Dynamic recrystallization in high-strain, high-strain-rate plastic deformation of copper. *Pergamon Acta metall, mater* **42** (1994).
11. Wu, X. Yang, M., Jiang, P., Wang, C., Zhou, L., Yuan, F., Ma, *E.* Deformation nanotwins suppress shear banding during impact test of CrCoNi medium-entropy alloy. *Scr. Mater.* **178**, 452–456 (2020).
12. Walley, S. M. Shear localization: A historical overview. In *Metallurgical and Materials Transactions A: Physical Metallurgy and Materials Science* vol. 38 A 2629–2654 (2007).
13. Meyers, M. A., Andrade, U. R. & Chokshi, A. H. *The Effect of Grain Size on the High-Strain, High-Strain-Rate Behavior of Copper*.
14. Karantza, K. D. & Manolakos, D. E. A review on the adiabatic shear banding mechanism in metals and alloys considering microstructural characteristics, morphology and fracture. *Metals* **13**. https://doi.org/10.3390/met13121988 (2023).
15. Jia, D., Ramesh, K. T. & Ma, E. Effects of nanocrystalline and ultrafine grain sizes on constitutive behavior and shear bands in iron. *Acta Mater.* **51**, 3495–3509 (2003).
16. Li, J., Li, Y., Huang, C., Suo, T. & Wei, Q. On adiabatic shear localization in nanostructured face-centered cubic alloys with different stacking fault energies. *Acta Mater.* **141**, 163–182 (2017).
17. Asgari, S., El-Danaf, E., Kalidindi, S. R. & Doherty, R. D. *Strain Hardening Regimes and Microstructural Evolution during Large Strain Compression of Low Stacking Fault Energy Fcc Alloys That Form Deformation Twins*. vol. 28 (1997).
18. Paul, H., Driver, J. H., Maurice, C. & Jasieński, Z. Shear band microtexture formation in twinned face centred cubic single crystals. *Mater. Sci. Eng. A* **359**, 178–191 (2003).
19. Paul, H., Driver, J. H. & Jasienskijasienski, Z. Shear banding and recrystallization nucleation in a Cu-2%Al alloy single crystal. *Acta Mater.* **50**. www.elsevier.com/locate/actamat(2002).
20. Long, B. Z. et al. Enhanced dynamic mechanical properties and resistance to the formation of adiabatic shear band by Cu-rich nano-precipitates in high-strength steels. *Int. J. Plast.* **138**, (2021).
21. Morii, K. & Nakayama, Y. *The effect of precipitates on shear band formation in rolled single crystals of AL-2%CU Alloy*. vol. 20 (1986).
22. Yiadom, S. B., Khan, A. K. & Bassim, N. Effect of microstructure on the nucleation and initiation of adiabatic shear bands (ASBs) during impact. *Mater. Sci. Engineering: A*. **615**, 373–394 (2014).
23. Sarmast-Ghahfarokhi, S., Midawi, A. R. H., Yasnogorodski, V., Benoit, M. J. & Zhou, Y. N. Improvement of the mechanical performance of ZnAlMg coated steel brazed joints through precipitation-based strengthening. *Mater. Sci. Eng. A* **145657**. https://doi.org/10.1016/j.msea.2023.145657 (2023).
24. Sarmast-Ghahfarokhi, S. et al. Investigating the microstructural evolution and interfacial morphology of laser- and arc-brazed ZnAlMg coated steel. *J. Mater. Process. Technol.* **316**, 1 (2023).
25. Vaidyanathan, R., Dao, M., Ravichandran, G. & Suresh, S. Study of mechanical deformation in bulk metallic glass through instrumented indentation. *Acta mater.* **1**, 49 (2001).
26. Ramamurty, U., Jana, S., Kawamura, Y. & Chattopadhyay, K. Hardness and plastic deformation in a bulk metallic glass. *Acta Mater.* **53**, 705–717 (2005).
27. Xie, S. & George, E. P. Hardness and shear band evolution in bulk metallic glasses after plastic deformation and annealing. *Acta Mater.* **56**, 5202–5213 (2008).
28. Manda, P., Chakkingal, U. & Singh, A. K. Hardness characteristic and shear band formation in metastable β-titanium alloys. *Mater. Charact.* **96**, 151–157 (2014).
29. Lu, Y. M. et al. Shear-banding Induced indentation size effect in metallic glasses. *Sci. Rep.* **6** (2016).
30. Zhang, H., Jing, X., Subhash, G., Kecskes, L. J. & Dowding, R. J. Investigation of shear band evolution in amorphous alloys beneath a Vickers indentation. *Acta Mater.* **53**, 3849–3859 (2005).
31. Subhash, G. Shear band patterns in metallic glasses under static indentation, dynamic indentation, and scratch processes. *Metall. Mater. Trans. A* **38**, 2936–2942 (2007).
32. Sharma, A., Nandam, S. H., Hahn, H. & Prasad, K. E. On the differences in shear band characteristics between a binary Pd-Si metallic and nanoglass. *Scr. Mater.* **191**, 17–22 (2021).
33. Wang, S. et al. The evolution of shear bands in Ta-2.5 W alloy during cold rolling. *Mater. Sci. Eng. A*. **726**, 259–273 (2018).
34. Boakye-Yiadom, S. & Bassim, N. Microstructural evolution of adiabatic shear bands in pure copper during impact at high strain rates. *Mater. Sci. Engineering: A*. **711**, 182–194 (2018).
35. Hong, C. S., Tao, N. R., Huang, X. & Lu, K. Nucleation and thickening of shear bands in nano-scale twin/matrix lamellae of a Cu-Al alloy processed by dynamic plastic deformation. *Acta Mater.* **58**, 3103–3116 (2010).
36. Keryvin, V. Indentation of bulk metallic glasses: relationships between shear bands observed around the prints and hardness. *Acta Mater.* **55**, 2565–2578 (2007).
37. Midawi, A. R. H., Simha, C. H. M., Gesing, M. A. & Gerlich, A. P. Elastic-plastic property evaluation using a nearly flat instrumented indenter. *Int. J. Solids Struct.* **104–105**, 81–91 (2017).
38. Chen, T. & Li, J. Modelling the shear banding in gradient nano-grained metals. *Nanomaterials* **11** (2021).
39. Nesterenko, V. F., Bondar, M. P. & Ershov, I. V. *Instability of Plastic flow at Dynamic pore Collapse*in 1173–1176 (AIP Publishing, 2008). https://doi.org/10.1063/1.46472.
40. Li, Z. Zhao, S., Wang, B., Cui, S., Chen, R., Valiev, R. Z., & Meyers, M. *A*. The effects of ultra-fine-grained structure and cryogenic temperature on adiabatic shear localization in titanium. *Acta Mater* **181**, 408–422 (2019).
41. Yang, H., Zhang, J. H., Xu, Y. & Meyers, M. A. Microstructural characterization of the shear bands in Fe-Cr-Ni single crystal by EBSD. *J. Mater. Sci. Technol.* **24** (2008).
42. Huang, C. X., & Li, S. X. Deformation twinning in polycrystalline copper at room temperature and low strain rate. *Acta Mater.* **54**, 655–665 (2006).
43. Goto, M., Han, S. Z., Yakushiji, T., Lim, C. Y. & Kim, S. S. Formation process of shear bands and protrusions in ultrafine grained copper under cyclic stresses. *Scr. Mater.* **54**, 2101–2106 (2006).
44. Pande, C. S. & Cooper, K. P. Nanomechanics of Hall-Petch relationship in nanocrystalline materials. *Prog. Mater. Sci.* **54**, 689–706. https://doi.org/10.1016/j.pmatsci.2009.03.008 (2009).

45. Jo, M. C. et al. *Understanding of adiabatic shear band evolution during high-strain-rate deformation in high-strength armor steel. J. Alloys Compd.* **845**, *(* (2020).
46. Chen, J. et al. Adiabatic shear band development and following failure in 316L fabricated by an additive manufacturing process. *Mater. Sci. Engineering: A* **811**, (2021).
47. Xu, Y., Zhang, J., Bai, Y. & Meyers, M. A. Shear localization in dynamic deformation: Microstructural evolution. *Metall. Mater. Trans. Phys. Metall. Mater. Sci.* **39 A**, 811–843 (2008).
48. Malow, T. R., Koch, C. C., Miraglia, P. Q. & Murty, K. L. Compressive Mechanical Behavior of Nanocrystalline Fe Investigated with an automated ball indentation technique. *Mater. Sci. Eng.* **252** (1998).
49. Sundararajan, G. & Tirupataiah, Y. The localization of plastic flow under dynamic indentation conditions: I. Experimental results. *Acta Mater.* **54**, 565–575 (2006).
50. Li, N. et al. Localized amorphism after high-strain-rate deformation in TWIP steel. *Acta Mater.* **59**, 6369–6377 (2011).
51. Nie, Y. et al. In situ Observation of Adiabatic Shear Band formation in aluminum alloys. *Exp. Mech.* **60**, 153–163 (2020).
52. Cerreta, E. K. et al. Microstructural examination of quasi-static and dynamic shear in high-purity iron. *Int. J. Plast.* **40**, 23–38 (2013).
53. Cowie, J. G., Azrin, M. & Olson, G. B. *Microvoid Formation during Shear Deformation of Ultrahigh Strength Steels.*
54. Cowie, J. G. & Tuler, F. R. *Flow localization Models-A review*. *Mater. Sci. Eng.* **95** (1987).
55. Peng, S., Wei, Y. & Gao, H. Nanoscale precipitates as sustainable dislocation sources for enhanced ductility and high strength. **117**, 5204–5209 (2020).
56. Liu, R. et al. Microstructure and formation mechanisms of nanotwins in the shear band in a FeCoNiCrMo0.2high-entropy alloy. *J. Mater. Res. Technol.* **20**, 2719–2733 (2022).
57. Ren, L. et al. Simultaneously enhanced strength and ductility in a metastable β-Ti alloy by stress-induced hierarchical twin structure. *Scr. Mater.* **184**, 6–11 (2020).
58. Li, X. et al. Twin-coupled shear bands in an ultrafine-grained CoCrFeMnNi high-entropy alloy deformed at 77K. *Mater. Res. Lett.* **10**, 385–391 (2022).
59. Ghatei-Kalashami, A., Khan, M. S., Goodwin, F. & Zhou, Y. N. investigating the mechanism of zinc-induced liquid metal embrittlement crack initiation in austenitic microstructure. *J. Mater. Sci.* **58**, 15314–15335 (2023).

Acknowledgements

The authors would like to thank the Natural Sciences and Engineering Research Council of Canada (NSERC), the Canada Research Chairs (CRC) program, and the International Zinc Association (Durham, NC, USA) for their financial support and for providing material to carry out this work.

Author contributions

Shadab Sarmast-Ghahfarokhi: Conceptualization, Methodology, Formal analysis, Investigation, Writing—Original Draft, Writing—Review and Editing; Ali Ghatei-Kalashami: Investigation, Methodology, contributed to the Discussion, Writing—Review and Editing; Adrian P. Gerlich: Contributed to the Discussion, Writing—Review and Editing; Michael J. Benoit: Supervision, Writing—Review and Editing; Y. Norman Zhou: Supervision, Funding acquisition, Writing—Review and Editing, Project administration.

Declarations

Competing interests

The authors declare no competing interests.

Additional information

Correspondence and requests for materials should be addressed to S.S.-G.

Reprints and permissions information is available at www.nature.com/reprints.

Publisher's note Springer Nature remains neutral with regard to jurisdictional claims in published maps and institutional affiliations.